



Investigation of graphene-coated Ag/AgCl electrode performance in surface electromyography measurement

Veysel Alcan^{a,*}, Ersan Harputlu^b, Cumhuri Gökhan Ünlü^c, Kasim Ocakoğlu^b, Murat Zinnuroğlu^d

^a Department of Electrical and Electronics Engineering, Faculty of Engineering, Tarsus University, Tarsus, Turkey

^b Department of Natural and Mathematical Sciences, Faculty of Engineering, Tarsus University, 33400, Tarsus, Turkey

^c Department of Biomedical Engineering, Faculty of Technology, Pamukkale University, Denizli, Turkey

^d Department of Physical Medicine and Rehabilitation, Faculty of Medicine, Gazi University, 06500, Ankara, Turkey

ARTICLE INFO

Keywords:

Surface electromyography
Graphene
Nanomaterial
Sensor
Electrode
Nerve conduction studies
Biopotential

ABSTRACT

Conventional silver-silver chloride (Ag/AgCl) electrodes are widely used for recording surface electromyography (sEMG) with a conductive gel. However, for long-term sEMG recording, the gel has some disadvantages that cause high impedance. Therefore, the dry electrodes have been alternatively purposed to overcome these disadvantages. Recently, the nanomaterial-based dry electrodes have been developed for long term electrophysiological signal recording. In the present study, we aimed to develop a graphene-coated Ag/AgCl electrode for long-term recording. We transferred single layer graphene (SLG) on the Ag/AgCl electrode surface by using chemical vapor deposition and confirmed this process by Raman scattering spectroscopy and scanning electron microscopy. We then compared the graphene-coated Ag/AgCl and conventional Ag/AgCl electrodes by evaluating median motor nerve conduction studies (mNCS) and their impedance. The charge transfer resistance (R_{ct}) for the Ag/AgCl electrode (4170 Ω) was much higher than graphene-coated Ag/AgCl electrode ($R_{ct} = 24.6 \Omega$). For median mNCS measurements without gel, the graphene-coated Ag/AgCl electrode provided a better amplitude of distal and proximal compound muscle action potential (28.3 mV and 25.8 mV, respectively) than the Ag/AgCl electrode (21.8 mV and 20.9 mV, respectively). Consequently, the present study suggests promising results in terms of the usability of graphene-coated Ag/AgCl electrodes for long-term monitoring and wearable systems applications of sEMG. In future studies, we aim to investigate clinical applicability of graphene-coated sEMG electrodes that include extended clinical settings and larger study population.

1. Introduction

Surface Electromyography (sEMG) is the gold-standard technique that measures voluntary or involuntary muscle activities. It provides very useful and important quantitative electrophysiological information for the diagnosis of the disorders, evaluation of the treatments, and various aspects of the person's health status and functional limitation. sEMG signals are conventionally recorded using surface electrodes, which are typically placed on the skin through a conductive gel. The quality of sEMG signals depend mainly on electrode-skin interactions and signal-to-noise ratio (Farina et al., 2004). The electrode-skin interaction is one of the important sources of noise among several sources, such as environmental noises, movements, skin state, amplifiers. The fluctuations in the impedance between the electrode and the skin cause

changes in long-term recording the amplitude of noise as result of the electrode-skin interaction, which converts the ionic currents from the muscles into electrical currents (Fernández and Pallás-Areny, 1992; Huigen et al., 2002). Therefore, the performance of sEMG electrodes also depends considerably on the electrode-skin impedance. The low electrode-skin impedance cause so high the electrical conductivity that increases the quality of sEMG signal (Mcadams et al., 1996; Rosell et al., 1988). Therefore, the gel is commonly used in sEMG records to facilitate the electrochemical reactions (Rosell et al., 1988; Webster, 2010). For the short-medium term recordings (the vast majority of the applications), gel has the advantage of reducing electrode-skin impedance. However, for the long-term recording, gel has some disadvantages that cause high impedance because of skin irritations, bacterial growth in particular for prolonged use, gel dehydration over time, fixing

* Corresponding author. Department of Electrical and Electronics Engineering, Faculty of Engineering, Tarsus University, 33400, Tarsus/Mersin, Turkey.
E-mail address: alcanveysel@tarsus.edu.tr (V. Alcan).

<https://doi.org/10.1016/j.biosx.2022.100193>

Received 5 June 2022; Received in revised form 2 July 2022; Accepted 4 July 2022

Available online 16 July 2022

2590-1370/© 2022 The Author(s). Published by Elsevier B.V. This is an open access article under the CC BY-NC-ND license (<http://creativecommons.org/licenses/by-nc-nd/4.0/>).

electrodes to prevent the gel from leaking out, and signal degradation with sweat. As a result, the signal quality decreases. (Searle et al., 2000; Jung et al., 2012; Baek et al., 2008). To overcome these difficulties, researchers tend to investigate alternative dry electrodes long-term recording (Mühlsteff and Such, 2004; Laferriere et al., 2011; Myers et al., 2015; Posada-Quintero et al., 2016; Shahandashti et al., 2019). Although dry electrodes have showed good performance when compared conventional Ag/AgCl electrodes with gel (Laferriere et al., 2011; Posada-Quintero et al., 2015, 2016), these electrodes have also some disadvantages, such as high contact impedance and motion artifacts (Jung et al., 2012; Myers et al., 2015). Therefore, to detect the high-quality sEMG signals, one effective method is to develop novel electrode material with low contact impedance.

Recently, the advances in material science have led to improving the electrode structure for better conductivity of the electrode-skin interface. The application of nanomaterial-based dry electrodes has received much more attention for bipotential measurements (Baek et al., 2008). Particularly, the graphene has been highly interested in biomedical applications due to its superior properties, for instance, the high electron mobility ($\sim 200,000 \text{ cm}^2 \cdot \text{V}^{-1} \cdot \text{s}^{-1}$), the high thermal conductivity ($5300 \text{ W m}^{-1} \cdot \text{K}^{-1}$), the high surface area to volume ratio ($2630 \text{ m}^2/\text{g}$), the thinnest material (only 0.34 nm thick), the faster moving electrons ($\sim 10^6 \text{ m/s}$), and the better conductor of electricity (resistivity of $10^{-6} \Omega \text{ cm}$) in any material (Yun et al., 2017; Yapici et al., 2015; Celik et al., 2016; Hitscherich et al., 2018; Lou et al., 2016). In the present study, we aimed to develop a graphene-coated Ag/AgCl electrode to improve the conductivity of the conventional Ag/AgCl electrode. We chose single-layer graphene because its structure does not affect the contact surface area between the electrode and the skin while it can increase the conductivity. We evaluated quantitatively graphene-coated Ag/AgCl electrodes, by using median motor nerve conduction studies (NCSs) and measurement of skin-electrode impedance.

2. Materials and methods

2.1. Graphene-based electrode fabrication

We coated single-layer graphene onto the Ag/AgCl electrodes after graphene growth on a metallic substrate and transfer processes. Single-layer graphene (SLG) was produced on copper (Cu) foil by using chemical vapor deposition (CVD). We transferred SLG ($1 \times 1 \text{ cm}^2$) onto the Ag/AgCl electrode substrate as the following procedure in Fig. 1. The graphene was produced utilizing hydrogen (H_2) and methane (CH_4)

gases based on the CVD growth procedure, similar to those used elsewhere in the literature on copper (Cu) substrates to yield monolayer graphene films. To get the graphene layer from the copper surface, firstly Graphene/Cu surface was coated with a polymethyl methacrylate (PMMA) support layer. In this procedure, the PMMA solution was spin-coated onto the sample at 4000 rpm . PMMA/SLG/Cu electrode was kept at a hot plate (90°C) for 10 min to dry, then the Cu substrate under the graphene film was etched in an iron nitrate solution. After the etching process, PMMA/SLG layer was cleaned in ultra-pure water many times (Reina et al., 2008; Strudwick et al., 2014). To transport the graphene layer to the Ag/AgCl electrode having a hole surface, we cut the PMMA/SLG/Cu piece in a suitable shape (rounded, 10 mm diameter), then we transferred this piece to the Ag/AgCl electrode (Fig. 2a). Lastly, to remove the PMMA layer on the graphene surface, the electrode was kept in dry acetone for 30 min . The presence of the graphene layer on the Ag/AgCl electrode surface was checked by using Raman scattering spectroscopy. Investigating the surface morphology of the SLG-Ag/AgCl

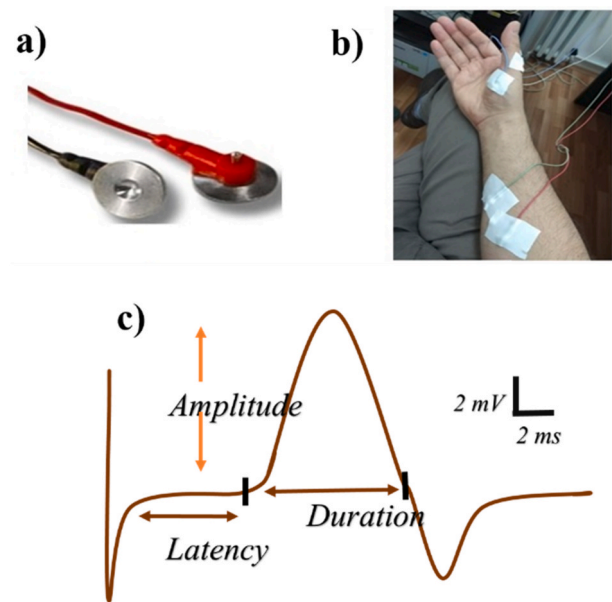


Fig. 2. Experimental settings. a) Disc type Ag/AgCl electrode. b) Protocol for motor median NCS test. c) CMAP morphology.

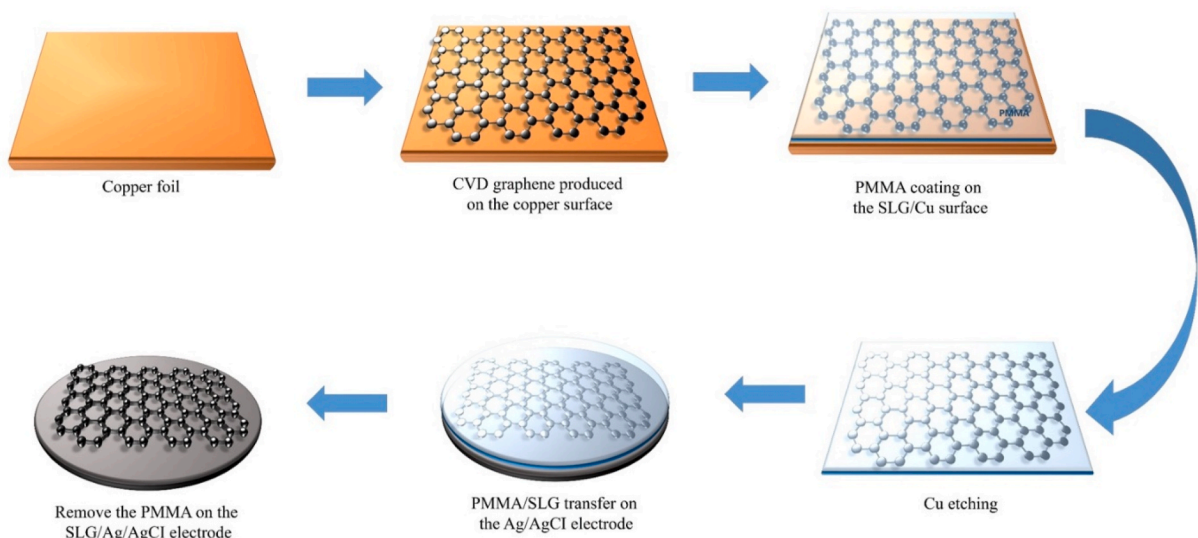


Fig. 1. Schematic diagram of the wet transfer of single-layer graphene from Cu substrate to Ag/AgCl electrode.

disk was confirmed by scanning electron microscopy (SEM).

We recorded field emission scanning electron microscopy images by using a Zeiss/Supra 55 FE-SEM (Carl Zeiss NTS GmbH, Oberkochen, Germany) microscope. The SEM analysis confirmed that the SLG completely covers the Ag/AgCl electrode surface without any wrinkles during the transferring process. The structural properties of CVD graphene transferred on the Ag/AgCl electrode were characterized by Raman scattering spectroscopy (Raman spectrum was recorded by using a WITec alpha300 Raman microscope, Germany). Thanks to this method could be determined the number of graphene layers and whether any defects occurred electrode surface during the transfer method of the SLG to the selected electrode surface.

2.2. Experimental protocol and signal processing

sEMG is a random, nonstationary, and complex signals and many physiological and non-physiological factors can affect its morphology such as anatomic, recording system, geometrical, physical, fiber membrane properties, and motor unit properties (Farina et al., 2004). In our tests, we did not record muscle contractions (dynamic and isometric) with and without any resistance to keep minimal effects of the subjective measurement because it could be very difficult to maintain the same amount of contraction and the same conditions while comparing two signals from one subject or two subjects. For evaluating the performance of the electrodes recording sEMG signals, we used motor NCS to obtain evoked sEMG signals by providing the same level of muscle stimulation in each trial. We stimulated only the median motor nerve under investigation and recorded the response generated by that nerve only (selectivity concept), using a bipolar electric stimulator. This stimulator consists of a cathode and anode surface electrodes sending a direct current to the nerve.

For our preliminary methodological study, one of co-author in the present study, who was a medical doctor (age=32 years old, height=190 cm, and weight = 80 kg), was enrolled in the experimental study. Tests were performed on the same person in the same session. NCS tests were conducted with a Viasys Medelec Synergy sEMG device (Medelec, Surrey, UK). Filter settings were 20 Hz low pass and 2 kHz high pass. Sweep speed and sensitivity were set as 1 ms/division and 20 μ V/div, respectively. These settings were increased if needed. Skin temperature was maintained at 32 °C and room temperature between 22 °C and 25 °C. All electrodes were 10 mm in diameter (Fig. 2b). The position of the electrodes was marked. Thus, the same distance was ensured while changing graphene-coated Ag/AgCl and Ag/AgCl electrodes. The distance between the active stimulating and recording electrodes was 5 cm according to standard clinic protocols (Alcan et al., 2020). The distance between the stimulator electrodes was 3 cm. During the specified time, we stimulated the nerve bypassing the current of the assigned intensity through the nerve. Stimulus intensity and duration were some of the basic parameters in NCSs. We used stimulation intensity between 10 and 30 mA and stimulus duration was set as 0.1 ms (Jablecki et al., 2002). To make the measurement accurate and repeatable, we added a value of 10–15% on the maximum intensity detected. We determined this stimulation intensity achieved as the level of supramaximal stimulation in median motor NCS. Stimulation intensity thus was 10–30 mA.

For the median motor NCS test, we placed the active recording electrode over the end-plate zone (the belly of the muscle) of the abductor pollicis brevis (APB) muscle. The reference electrode was placed nearby in an electrically quiet area (tendon). We considered the belly-tendon principle. We placed the ground electrode between the stimulating and recording electrodes. Subsequently, we stimulated the median nerve was using surface electrodes at the wrist (distal) and elbow (proximal) sites, yielding two separate motor responses. We then recorded distal compound muscle action potential (CMAP) and proximal CMAP (in Fig. 2c). Whenever the motor response had a triphasic appearance, we repositioned the active recording electrode. Each record

was carried out in 1–2 min. The interval between records took 2–3 min, which included standard protocols such as skin preparation (cleaning and abrasion), electrode connections, and a stimulator. In this way, we tried to minimize the changes in skin impedance due to the skin surface. We measured latency and amplitude from motor responses. Peak to peak amplitude of the CMAP was measured from the trough of the peak of the first negative component to the peak of the positive component in the millivolt (mV). The latency of the CMAP generated with distal stimulation was referred to as the median motor distal latency (wrist), whereas the latency of the CMAP generated with proximal stimulation was referred to as the proximal (elbow) latency. The latency value was taken from the onset of the negative phase and measured in milliseconds (ms). We repeated these tests three times and we calculated mean values.

2.3. Electrical and electrochemical properties

The impedance of the skin-electrode interface plays an important role in the conductivity of sEMG signals. To better understand the impedance behavior between the skin and the electrode, some electrical models were suggested for the skin-electrode interface (Taji et al., 2018).

Fig. 3 shows a typical electrode-skin interface and its electrical model.

In Fig. 3a, E_{he} represents the potential difference between the skin and the electrode. C_d represents the capacitance that may occur to the charges located between the electrode and the skin double layer. R_d represents the leakage resistance that may occur to the charges transfer between the skin and electrodes. R_g resistance series are related to the conductive gel. Dry electrodes are characterized by the absence of wet adhesive at the electrode-skin interface. After the electrode is placed, the skin starts to produce sweat. In such a case, sweat aids in electrical conduction as it is ionically conductive. It also increases the adhesion of the electrode to the skin surface due to surface tension. It behaves similarly to the case of the conductive gel in the wet electrode. In Fig. 3b, C_g capacitor indicates the presence of air bubbles or gaps between the dry electrode and the skin. C_g and R_g is modeled with the parallel-connected in the electrode and skin interface. R_e represents the resistance of the epidermis. C_e represents the capacitance induced by the nonconductive stratum corneum layer. The stratum corneum has a high resistance to the electrical current due to the presence of dead skin cells. R_{sub} represents the overall resistance of the tissue underneath the epidermis layer. The equation of the impedance for the electrode-skin interface is the following:

$$Z_c = R_s + \frac{R_d}{1 + j2\pi f C_d} \quad (1)$$

where f is the frequency (Hz).

We performed electrochemical measurements of both graphene-coated Ag/AgCl electrode and conventional Ag/AgCl electrodes by using Electrochemical Impedance Spectroscopy (EIS). Standard electrochemical cell configuration was set with an Ag/AgCl reference electrode, a platinum counter electrode, and the Ag/AgCl electrode before and after graphene transfer as a working electrode, connected with IviumStat electrochemical system. All the electrochemical measurements were performed at room temperature, in 0.1 M KCl mixed with 5.0 mM $K_3[Fe(CN)_6]$ and 5.0 mM $K_4[Fe(CN)_6]$. The electrochemical impedance spectra (EIS) were recorded in a frequency range from 0.1 Hz to 100 kHz, under open circuit potential (OCP). We used Nyquist plots to examine the EIS measurements and represented them with the equivalent electric circuit.

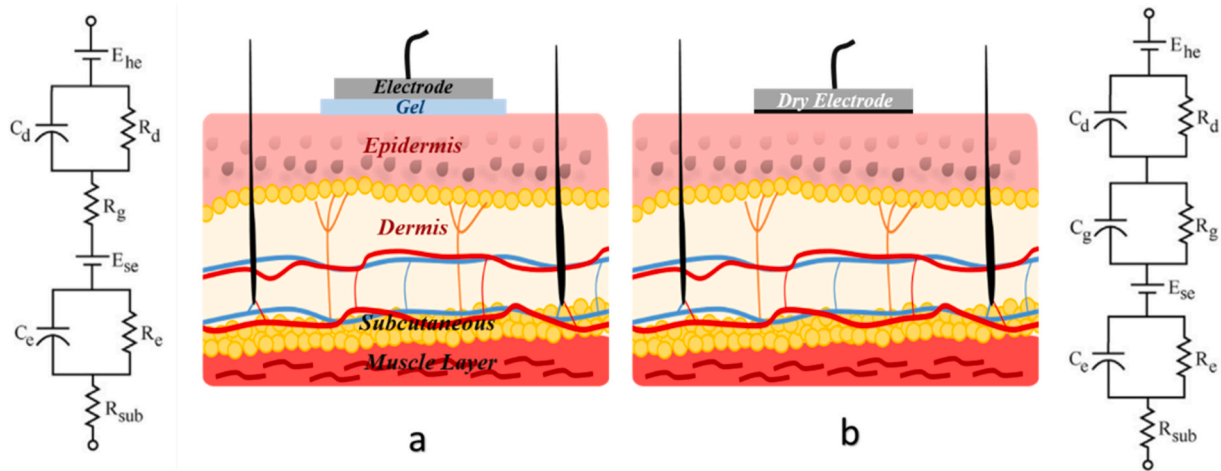


Fig. 3. Equivalent circuit model of the skin-electrode interface: (a) Wet electrode, and (b) Metal dry electrode.

3. Results

3.1. SEM and Raman spectroscopy of graphene-coated Ag/AgCl electrode

Due to the highly transparent structure of SLG, the area occupied by the Ag/AgCl electrode surface can be seen easily through SEM images as shown in Fig. 4.

In Fig. 4a and b, SLG is covered on the electrode surface fully. Moreover, It is also seen that the stresses (arrow marks and areas within

the circles) on some point particles on the Ag/AgCl electrode surface are formed by SLG. The presence of the site SLG layer on the surface was determined by Raman spectroscopy. The surface smoothed by the graphene coating can provide better skin-electrode contact. That is, this process contributes to better sEMG signal recording. Fig. 4c presents a typical Raman spectrum of the SLG on the Ag substrate. Due to the width of the graphene-coated electrode surface area, the Raman spectrum has obtained an average of different areas of the graphene-coated electrode surface. Raman spectroscopy is capable of determining the number of

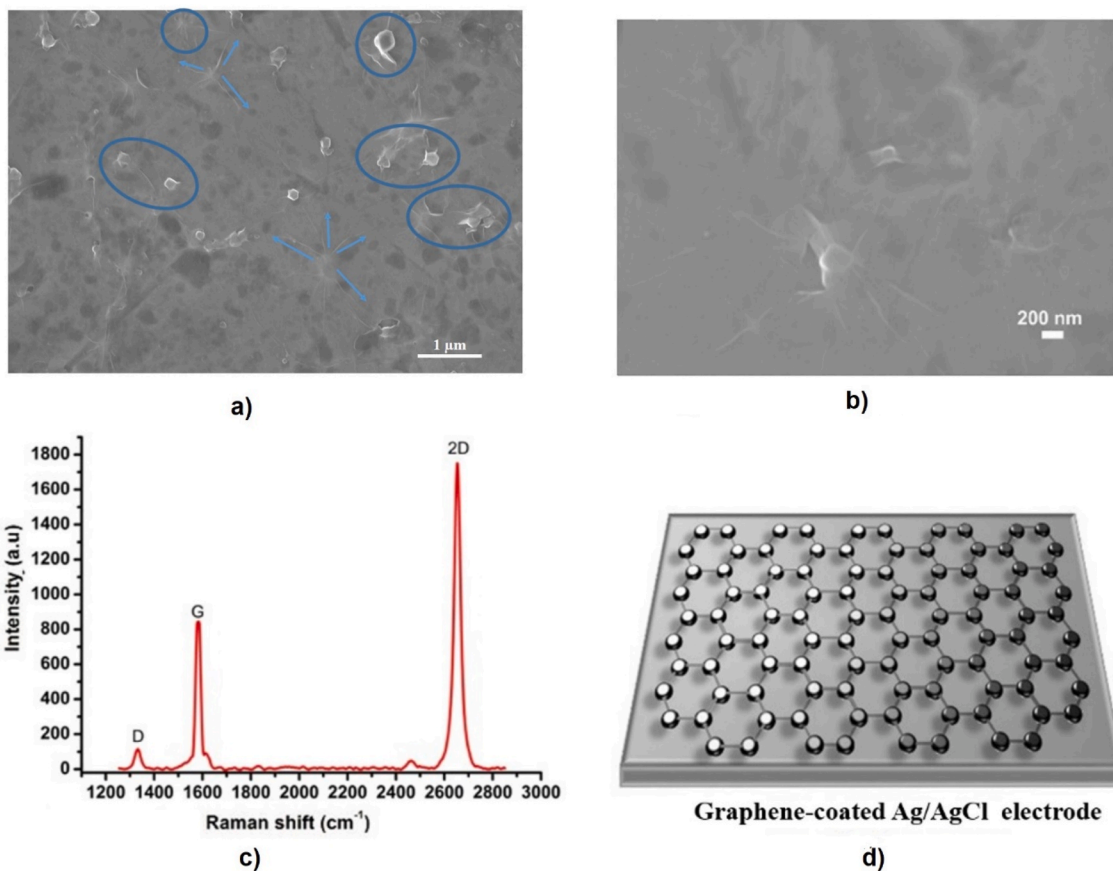


Fig. 4. SEM images of graphene-coated Ag/AgCl electrode. a) Particles on the Ag/AgCl electrode with arrow marks and areas within the circles. b) Different magnification with bigger size. (c) Average Raman spectrum of a graphene-coated Ag/AgCl electrode substrate. (d) Schematic diagram of graphene-coated Ag/AgCl electrode.

layers of graphene by positioning and shaping three important bands (D, G, 2D bands). The D, G, and 2D peaks were identified following excitation of SLG on Ag substrate at 488 nm and were determined at 1345, 1581, and 2672 cm^{-1} (see Fig. 4c). The ratio between the D band and the G band, which is frequently used to evaluate the quality of graphene, was 0.13, which implies a low number of defects in the π -system and good quality of SLG transferred onto the Ag substrate. The measurement of full width at half maximum (FWHM) was obtained at 16.1 and 30.12 cm^{-1} for G and 2D bands. Also, a very sharp and symmetrical 2D band in conjunction with the high 2D/G peak ratio of 2.8 confirms the single layer formation of graphene in our system. Fig. 4d represents a schematic diagram of the graphene-coated surface.

3.2. Electrochemical properties of graphene-coated Ag/AgCl and Ag/AgCl electrodes

Nyquist plots show the imaginary impedance (Z'') versus the real impedance (Z') in Fig. 5. We determined the charge transfer resistance (R_{ct}) from the semicircular curve corresponding to the high frequencies. Conventional Ag/AgCl electrode was much higher R_{ct} (4170 Ω) than graphene-coated Ag/AgCl electrode ($R_{ct} = 24.6 \Omega$).

3.3. NCS results

We quantitatively compared graphene-coated Ag/AgCl and conventional Ag/AgCl electrodes by evaluating amplitude and latency values measured from NCS tests. Table 1 shows the result of comparison median motor NCS tests.

In Table 1, the graphene-coated Ag/AgCl electrode without gel provided better amplitude for distal CMAP and proximal CMAP (28.3 mV and 25.8 mV, respectively) than the conventional Ag/AgCl electrode (23.2 mV and 22.9 mV, respectively). But conversely, Ag/AgCl electrode with gel provided better amplitude for distal CMAP and proximal CMAP (24.6 mV and 23.9 mV, respectively) than the graphene-coated Ag/AgCl electrode (21.8 mV and 20.9 mV, respectively). In latency measurements, the graphene-coated Ag/AgCl electrode without gel had shorter latency values (2.60 ms for distal CMAP) than the conventional Ag/AgCl electrode without gel (2.85 ms for distal CMAP). Similarly, the graphene-coated Ag/AgCl electrode with gel had shorter latency (2.40 ms for distal CMAP) than the conventional Ag/AgCl electrode with gel (2.55 ms for distal CMAP). Both graphene-coated Ag/AgCl and Ag/AgCl electrodes with gel and without gel had the same latency values of proximal CMAP (7.35 ms and 7.30 ms respectively).

4. Discussion

We evaluated performance of graphene-coated Ag/AgCl electrode with gel and without gel by comparing conventional Ag/AgCl electrode. Our results showed that SLG provided better charge transfer performance and excellent conductivity.

Long-term recording of sEMG signals has increasingly become attractive for health monitoring, diagnosis, and treatment. Although conventional Ag/AgCl electrodes are commonly used with gel in sEMG recording, the gel itself has also some disadvantages for long-term recording that cause high impedance at the electrode-skin interface because of skin irritations, bacterial growth for prolonged use, dehydration over time, and signal degradation with sweat. Therefore, the previous studies tend to research on developing dry electrodes with flexibility, measurement accuracy, high signal quality, and clinical applicability (Laferrriere et al., 2011; Posada-Quintero et al., 2015; Mühlsteff and Such, 2004). The existence of conductive gel on the Ag/AgCl electrodes produced low skin-electrode impedance (Z_e) values (Meziane et al., 2013; Albulbul, 2016). In the present study, when comparing conventional Ag/AgCl electrodes, the graphene-coated Ag/AgCl electrode without gel showed high CMAP amplitude due to low skin-electrode impedance while graphene-coated Ag/AgCl electrodes with gel showed low amplitude value. Our results show that conductive gel could not be useful to improve the conductivity of nanomaterials-based electrodes. One possible reason could be ion transfer between the conductive gel and the graphene-coated Ag/AgCl electrode surface that became at low speed and interaction through the charges transfer between the skin and the graphene-coated surface. R_s values of the electrodes could be varied because of material diversity but R_d values depend on the patient's skin properties and preparations. According to a previous study on the resistivity between the electrode and the conductive gel, if the resistivity of the conductive gel was low, the current tended to concentrate just below the ECG electrode surface. On the other hand, if the electrode had a higher resistivity than the gel, the current lines just tended to flow in the gel (Grassini, 2013) [30]. In our study, graphene without gel showed low electrode-skin impedance, which was likely due to higher electron-ion exchanges that were linked with high mobility of ions across the highly resistant skin layer and high electron-ion exchange at the graphene-coated part of the electrode. As a result of this, the sEMG signal amplitude could be improved due to the strong conductivity between the electrode and the skin. Our results also confirmed previous studies. Lou et al. developed a graphene-based dry flexible ECG electrode and they reported that the graphene electrode was able to acquire the typical properties of human ECG signals with an

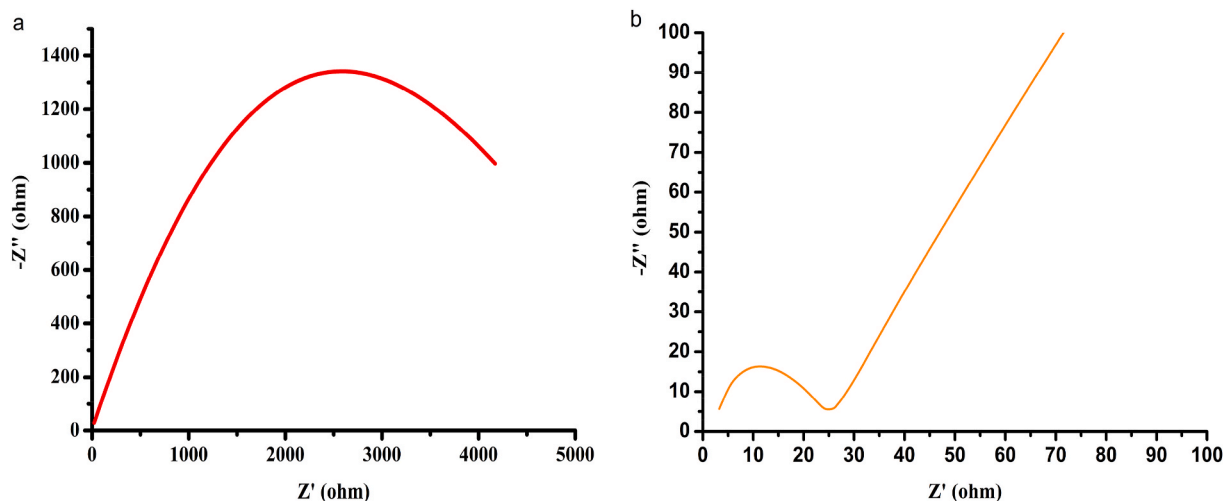


Fig. 5. Nyquist plot of Ag/AgCl working electrode (a) Graphene coated Ag/AgCl electrode, (b) electrolyte solution including 0.1 M KCl mixed with 5.0 mM $\text{K}_3[\text{Fe}(\text{CN})_6]$ and 5.0 mM $\text{K}_4[\text{Fe}(\text{CN})_6]$.

Table 1

Comparison of median motor NCS results between graphene-coated Ag/AgCl electrode and conventional Ag/AgCl electrode.

Electrode Type	With gel				Without gel			
	Distal CMAP		Proximal CMAP		Distal CMAP		Proximal CMAP	
	Lat (ms)	Amp (mV)	Lat (ms)	Amp (mV)	Lat (ms)	Amp (mV)	Lat (ms)	Amp (mV)
Ag/AgCl	2.55	24.6	7.35	23.9	2.85	23.2	7.30	22.9
Graphene-coated Ag/AgCl	2.40	21.8	7.35	20.9	2.60	28.3	7.30	25.8

Lat=latency, Amp = peak to peak amplitude, APB = abductor pollicis brevis, CMAP=compound muscle action potential.

signal-noise ratio (SNR) in different states of motion (Lou et al., 2016). They also reported that it is useful for long-term ECG monitoring because of no degradation in the ECG signal quality over time. Similarly, Yapici et al. (2015) developed a graphene-coated textile electrode. They reported that the graphene-clad conductive electrode enables the acquisition of high-quality ECG signals. Yapici and Alkhidir (2017) also developed a fully-wearable medical garment for mobile monitoring of cardiac biopotentials from the wrists and the neck using graphene-functionalized textile electrodes. A comparison of the ECG recordings obtained from the wearable prototype against conventional wet electrodes indicated better conformity and spectral coherence among the two signals. For long term wearable ECG monitoring, Celik et al. (2016) developed a graphene-based electrode by coating graphene on top of a metallic layer of an Ag/AgCl electrode which is similar to our study in terms of electrode material. Consequently, these previous studies developed different graphene based electrodes for ECG recording with different electrode constitution, geometric form, bandwidth, and noise. However, in terms of signal morphology, sEMG signals are different from ECG signals and are more complex, random, and non-stationary signals. ECG electrodes, particularly those for Holter recordings, often are larger than sEMG electrodes, which we intended to yield more local information. Moreover, electrodes used in monitoring EMG are generally smaller in diameter than those used in recording ECGs (Neuman, 1998). Therefore, our study was directed towards sEMG measurements by using small-sized electrodes (as extensively published, to avoid spatial averaging but possibly have a large contact surface to reduce impedance and noise (for more sensitivity and selectivity in terms of volume conductor). That's why we selected a reusable metal-disk electrode. On the other hand, although there are thousands of articles, hundreds of books and countless new applications in sEMG, its clinical acceptability in practice is not at the same level like as in ECG (Merletti and Muceli;2019) With the advent of wearable devices, there is a growing interest in dry electrodes for long-term remote recording and monitoring. However sEMG has not also reached good enough level as in ECG (Merletti and Muceli; 2019).

5. Conclusion

In the present study, we found that graphene-coated Ag/AgCl electrodes without gel had lower impedance and better electrochemical conductivity than the conventional Ag/AgCl electrode. Our results suggest promising results in terms of the usability of graphene-coated Ag/AgCl electrodes for long-term monitoring and wearable systems applications of sEMG. One of main limitation was the number of subjects for testing. We also did not directly evaluate the effect of the noise, artifact and power line interference due to our experimental protocol including electrically-induced contraction, which was a static condition with high SNR. In future studies, we aim to investigate clinical applicability of graphene-coated sEMG electrodes with different type and sized that include extended clinical settings and larger study population.

Funding statement

This research did not receive any specific grant from funding agencies in the public, commercial, or not-for-profit sectors.

CRediT authorship contribution statement

Veysel Alcan: Conceptualization, Investigation, Formal analysis, Writing – original draft, Writing – review & editing, for final manuscript. **Ersan Harputlu:** Methodology, Visualization, Investigation, Writing – original draft. **Cumhur Gökhan Ünlü:** Methodology, Visualization, Investigation. **Kasim Ocakoğlu:** Formal analysis, Validation, Writing – review & editing. **Murat Zinnuroğlu:** Formal analysis, Data collection and interpretation, Writing – review & editing.

Declaration of competing interest

The authors declare that they have no known competing financial interests or personal relationships that could have appeared to influence the work reported in this paper.

References

- Albulbul, A., 2016. *Bioengineering* 3, 20.
- Alcan, V., Kaya, H., Zinnuroğlu, M., Karataş, G.K., Canal, M.R., 2020. *Biomed. Tech.* 65, 61–71.
- Baek, J.Y., An, J.H., Choi, J.M., Park, K.S., Lee, S.H., 2008. *Sensor Actuator Phys.* 143, 423–429.
- Celik, N., Manivannan, N., Strudwicuk, A., Balachandran, W., 2016. *Nanomaterials* 6, 1–16.
- Farina, D., Merletti, R., Enoka, R., 2004. *J. Appl. Physiol.* 96, 1486–1495.
- Fernández, M., Pallás-Areny, R., 1992. In: 14th Annual International Conference of the IEEE Eng. Med. Biol. Soc. Paris.
- Grassini, S., 2013. *Corrosion and Conservation of Cultural Heritage Metallic Artefacts. European Federation of Corrosion (EFC) Series*, pp. 347–367.
- Hitscherich, P., Aphale, A., Gordan, R., et al., *J. Biomed. Mater. Res. A* 106, 2923–2933.
- Huigen, E., Peper, A., Grimbergen, C.A., 2002. *Med. Biol. Eng. Comput.* 40, 332–338.
- Jablecki, C.K., Andary, M.T., Floeter, M.K., Miller, R.G., Quarty, C.A., Vennix, M.J., et al., 2002. *Neurol. Now.* 11, 1589–1592.
- Jung, H.C., Moon, J.H., Baek, D.H., Lee, J.H., Choi, Y.Y., Hong, J.S., Lee, H.S., 2012. *IEEE Trans. Biomed. Eng.* 59, 1472–1479.
- Laferriere, P., Lemaire, E.D., Chan, A.D.C., 2011. *IEEE Trans. Instrum. Meas.* 60, 77–80.
- Lou, C., Li, R., Li, Z., Liang, T., Wei, Z., Run, M., Liu, X., 2016. *Sensors* 16, 1833.
- McAdams, E.T., Jossinet, J., Lackermeier, A., Risacher, F., 1996. *Med. Biol. Eng. Comput.* 4, 397–408.
- Merletti, R., Muceli, S., 2019. *J. Electromyogr. Kinesiol.* 49, 102363.
- Meziane, N., Webster, J.G., Attari, M., Nimunkar, A.J., 2013. *Physiol. Meas.* 34, R47–R69.
- Mühlsteff, J., Such, O., 2004. In: *Conf Proc IEEE Eng. Med. Biol. Soc.*, pp. 2212–2215, 2004.
- Myers, A.C., Huang, H., Zhu, Y., 2015. *RSC Adv.* 5, 11627–11632.
- Neuman, M.R., 1998. *Biopotential electrodes*. In: Webster, J.G. (Ed.), *Medical Instrumentation Application and Design*. Univ. of Wisconsin, Madison, pp. 289–291.
- Posada-Quintero, H.F., Reyes, B.A., Burnham, K., Pennace, J., Chon, K., 2015. *Ann. Biomed. Eng.* 43, 2374–2382.
- Posada-Quintero, H.F., Rood, R.T., Burnham, K., Pennace, J., Chon, K.H., 2016. *IEEE J. Transl. Eng. Health. Med.* 4, 2100209.
- Reina, A., Son, H., Jiao, L., Fan, B., Dresselhaus, M.S., Liu, Z., Kong, J., 2008. *J. Phys. Chem. C* 112, 17741–17744.
- Rosell, J., Colominas, J., Riu, P., Pallas-Areny, R., Webster, J., 1988. *IEEE Trans. Biomed. Eng.* 35, 649–651.
- Shahandashti, P.F., Pourkheyrollaha, H., Jahanshahi, A., Ghafoorifard, H., 2019. *Sens. Actuators A. Phys.* 295, 678–686.
- Strudwick, A.J., Weber, N.E., Schwab, M.G., Kettner, M., Weitz, R.T., Wunsch, J.R., et al., 2014. *ACS Nano* 9, 31–42.
- Taji, B., Chan, A.D.C., Shirmohammadi, S., 2018. *IEEE Trans. Instrum. Meas.* 67, 1900–1912.
- Webster, J.G., 2010. *IoT-Based Medical Devices*, 4th ed. John Wiley & Sons, New York, pp. 189–235.

Yapici, M.K., Alkhidir, T., 2017. *Sensors* 17, 875.

Yapici, M.K., Alkhidir, T., Samad, Y.A., Liao, K., 2015. *Sens. Actuators, B* 221, 1469–1474.

Yun, Y.J., Ju, J., Lee, J.H., Moon, S.H., Park, S.J., Kim, Y.H., et al., 2017. *Adv. Funct. Mater.* 27, 1701510–1701513.